universe

MDPI

Article

Effect of Ephemeris on Pulsar Timing and Navigation Accuracy Based on X-ray Pulsar Navigation-I Data

Yongtao Deng [1,2] and Shuanggen Jin [2,3,*]

[1] School of Communication and Information Engineering, Shanghai University, Shanghai 200444, China; dengyongtao@shao.ac.cn
[2] Shanghai Astronomical Observatory, Chinese Academy of Sciences, Shanghai 200030, China
[3] School of Surveying and Land Information Engineering, Henan Polytechnic University, Jiaozuo 454000, China
* Correspondence: sgjin@shao.ac.cn

Abstract: Solar system ephemeris is very important for pulsar timing and navigation. In order to explore the effect of different precision ephemerides on X-ray pulsar timing and navigation, the differences between timing and navigation results with four JPL Development Ephemerides based on the data of X-ray pulsar navigation-I (XPNAV-I) were compared and analyzed in this paper. For pulsar timing, the ephemeris has a systematic effect on time scale conversion (nanosecond difference), light-travel delay (millisecond difference) and timing residuals (microsecond difference), and the pulse profile phase can reflect the systematic deviation caused by different ephemerides in the timing calculation. The timing results show that it is necessary to compile the pulsar timing model based on the newer ephemeris. For navigation, based on the significant enhancement of pulse profile with orbit-dynamic (SEPO), the absolute error between simulation orbit and actual orbit is less than 2 km for each ephemeris, and the differences between simulation orbits are less than 1 km. The orbit position accuracy calculated by the ephemeris used in pulsar timing parameter calculation is the highest (DE200 in this paper), which explains the necessity of using a unified ephemeris in the calculation of timing and navigation with satisfying its internal self-consistency.

Keywords: X-ray pulsar navigation; pulsar timing; JPL DE ephemerides; XPNAV-I; satellite orbit determination

Citation: Deng, Y.; Jin, S. Effect of Ephemeris on Pulsar Timing and Navigation Accuracy Based on X-ray Pulsar Navigation-I Data. *Universe* **2022**, *8*, 360. https://doi.org/10.3390/universe8070360

Academic Editor: Giacomo Tommei

Received: 23 May 2022
Accepted: 23 June 2022
Published: 27 June 2022

1. Introduction

Pulsars are fast-rotating neutron stars in the universe with stable rotation periods, and the long-term stability is higher than that of the most precise atomic clock at present [1,2]. Since the first pulsar was discoved in 1967, the study of its physical properties has been a hot spot in the fields of radio astronomy and space high-energy radiation. Many radio-observation arrays and space high-energy radiation detectors around the world have long-term observation records of pulsars. The study of pulsars can be carried out to verify the relativistic effects, detect low-frequency gravitational waves and measure the mass of planets in the solar system [2–4]; At the same time, the pulsar time scale based on the ground radio pulsar timing array and spatial X-ray timing data is an important supplement to the integrated positioning, navigation and timing system (PNT), and the X-ray pulsar based navigation (XPNAV) with pulsar X-ray signal as the source is the most promising technology to achieve the long-time and high-precision Autonomous Navigation of deep space probe [5–11]. The research on pulsar timing and XPNAV is of great significance for space exploration by attracting the attention of the international community.

Since the concepts of pulsar timing and navigation were proposed in the 1970s, many researchers have demonstrated their specific implementation methods and feasibility by developing a set of relatively mature theoretical methods [9–15]. At the same time, related satellites in orbit experiments were also gradually carried out [7,11]. At present, the most effective is the Neutron-star Interior Composition ExploreR/Station Explorer for X-ray

Timing and Nav-igation Technology (NICER/SEXTANT) project carried out by NASA on the International Space Station in 2018, with a positioning error of better than 5 km [11]; Chinese institutions and researchers also carried out timing or satellite orbit determination experiments based on the observation data of the Insight-Hard X-ray Modulation Telescope (Insight-HXMT), the POLAR Gamma Ray Burst Polarimeter on the TianGong-2 Spacelab and the XPNAV-I [7,16–19]. The results verified the feasibility of X-ray pulsar navigation.

For a spacecraft flying in the solar system, to achieve pulsar navigation or improve its positioning and velocity measurement accuracy, precise solar system ephemeris is extremely necessary to correct the error terms caused by the relativistic effect and Doppler frequency shift [14]. At present, many institutions around the world have released the solar system ephemerides for different purposes, among which the Development Ephemerides (DE) released by NASA's Jet Propulsion Laboratory (JPL) has the highest comprehensive accuracy and is the most widely used [20]. Since JPL released the first ephemeris DE102 in 1981, 18 different versions of ephemerides have been released successively. Each ephemeris has certain differences in the observation data, inertial reference frame, time span, usage, etc., which leads to differences in the use of different ephemerides to calculate the position or speed of celestial bodies, and the position differences may reach tens of kilometers [21].

For pulsar navigation or timing, the effect of ephemeris on the accuracy of results is complex, and the noise components caused by different celestial errors are not independent but red noise coupled with each other. In recent years, there have still not been many studies in this field. Some scholars regard the ephemeris error as a geometric error, study its impact on the near-Earth satellite navigation and orbit determination system based on X-ray pulsar, and regard it as a part of the state vector processed by the filtering method [22,23]; Ning et al. [24] proposed a celestial/pulsar navigation method using time and ephemeris estimation. In order to eliminate the influence of the ephemeris errors of a planet's moon, the ephemeris of the planet's moons is augmented to the state and estimated in real time. Some of the latest studies also consider the influence of ephemeris on timing and positioning and propose improved methods [16,25]. In the research and application of pulsar navigation or timing, one of the important basic works is to determine the relevant pulsar rotation parameters and establish and update the navigation database in real time (especially for relatively young pulsars such as Crab pulsar, undetectable micro-jumps in pulsar rotation may cause serious "timing noise", so it is very necessary to obtain the latest timing parameters [26]). However, the parameters released in different periods or institutions may be fitted based on different ephemerides. When using these parameters, the internal self-consistency of the system should also be considered.

This paper aims at the problems and effects of ephemeris on pulsar navigation and timing. Firstly, the commonly used X-ray pulsar navigation and timing methods and data processing processes were summarized and analyzed, including time scale conversion, light-travel delay calculation, etc. On this basis, based on the observation data of XPNAV-I, the differences between the four commonly used JPL ephemerides DE200, DE405, DE421 and DE430 used in time scale conversion and light-travel delay calculation were calculated and compared, and the effect of ephemeris difference on pulse profiles and timing residuals were analyzed (For the description of XPNAV-I data and the four ephemerides, see reference [27] and Appendix A). Because there is no observation data that can realize navigation measurement at present, based on the orbit determination method of single pulsar observation data, the influence of each ephemeris on orbit determination was calculated and analyzed, and some suggestions on the use of ephemeris in pulsar navigation and timing are given according to the experimental results.

2. Effect of Ephemeris on Pulsar Timing

Using the high long-term stability of pulsar rotation to establish pulsar time to assist ground atomic time thereby improves the stability and reliability of ground time reference, which has a high practical value [8]. At the same time, pulsar timing is also the basis of pulsar navigation, and quality of timing results directly affects the accuracy of spacecraft

positioning and velocity measurement [7]. At present, the processing flow of observation data is generally the first to convert the detector's local recording time (Universal Time Coordinated(*UTC*) or Terrestrial Time(*TT*)) to the Barycentric Coordinate Time (*TCB*) or Barycentric Dynamical Time (*TDB*). The next step is to calculate the time delay from the detector to the solar system barycentric (SSB) at the photon arrival time according to the space-time coordinate information of the detector. Then, the phase of the corresponding time according to the pulsar's timing model is calculated, and the pulse profile is obtained by folding the discrete phase. Finally, the phase delay is obtained by cross-correlation operation with the standard pulse profile, and then the time of arrival (TOA) of the pulse is calculated [5,17]. The time scale conversion and time delay calculation can be expressed by the following formula:

$$t_{SSB} - t_{SC} = \Delta E + \Delta R + \Delta S + \Delta P \tag{1}$$

where t_{SSB} is the time when the photon or pulse reaches the SSB; t_{SC} is the local recording time of the detector; ΔE represents the Einstein delay caused by time scale transformation; ΔR represents Romer delay, i.e., the geometric delay between detector and SSB; ΔS represents the Shapiro delay, which is the relativistic effect delay caused by the gravity of all celestial bodies in the solar system; ΔP is the parallax delay caused by the change in spacecraft position. Since the subsequent experimental analysis is mainly based on the Crab observation data of XPNAV-I, for the observation data of a single pulsar, only the time delay between the detector and SSB needs to be considered, rather than the extrasolar delay such as a double pulsar system delay and interstellar delay. In addition, the standard delay formula should also include the dispersion delay of the solar system, but it has little impact on high-energy X-ray observation, and the delay generated by different ephemerides can be considered equal, so it is ignored.

2.1. Effect on Time Scale Conversion

Fields such as modern astronomy and geodesy use different time scales for different purposes. For pulsar observations, *TT* or *UTC* with the same scale as International Atomic Time(*TAI*) and only linear transformation is generally adopted; SSB is the inertial reference origin for the study of the motion of various celestial bodies in the solar system, and the corresponding time scale is *TCB* or *TDB*. For XPNAV-I satellite and JPL ephemeris, it is the conversion between *UTC* time and *TDB* time, and the standard conversion equation is as follows [5,28,29],

i. UTC→TAI:

$$TAI = UTC + LS \tag{2}$$

where *LS* represents the leap seconds between *UTC* and *TAI*, which can be obtained from the IERS Bulletin.

ii. *TAI*→*TT*:

$$TT = TAI + 32.184 \text{ s} \tag{3}$$

32.184 s is the origin difference between *TAI* and *TT*.

iii. *TT*→*TCG*:

$$TCG = TT + \left(\frac{L_G}{1 - L_G}\right) \times (JD_{TT} - T_0) \times 86,400 \tag{4}$$

where L_G represents the change rate of *TCG* relative to *TT*; *JD* represents Julian day; $T_0 = 2,443,144.5003725$, which is the origin of time (i.e., *TT* at 1977 January 1.0 *TAI*).

iv. TCG→TCB:

$$TCB - TCG = c^{-2}\left\{\int_{t_0}^{t}\left[\frac{v_e^2}{2} + U_{ext}(r_e)\right]dt + v_e \cdot r_{SC}\right\} + O\left(c^{-4}\right) \tag{5}$$

where v_e is the velocity vector of the Earth centroid relative to SSB, r_{SC} is the position vector of the satellite relative to the Earth centroid, and $U_{ext}(r_e)$ is the scalar potential of other

celestial bodies in the solar system except the Earth at the Earth centroid; $O\left(c^{-4}\right)$ represents the high-order delay term, and its calculation formula is

$$O\left(c^{-4}\right) = c^{-4}\left\{\int_{t_0}^{t}\left[-\frac{v_e^4}{8} - \frac{3v_e^2}{2}U_{ext}(r_e) + 4v_e \cdot U_{ext}(r_e) + \frac{1}{2}U_{ext}^2(r_e)\right]dt - \left[3U_{ext}(r_e) + \frac{v_e^2}{2}\right]v_e \cdot r_{SC}\right\} \quad (6)$$

where $U_{ext}(r_e)$ represents the vector potential corresponding to $U_{ext}(r_e)$; $O\left(c^{-4}\right)$ is less than the order of 10^{-16}, which can be ignored for calculations that do not require very high precision. The above transformations are in the first-order post-Newtonian system, and the asteroid correction term is considered. The integral operation is very time-consuming, and the following linear formula can be used for approximate calculation,

$$TCB - TCG = \frac{L_C \times (TT - T_0) + P(TT) - P(T_0)}{1 - L_C} + c^{-2}v_e \cdot r_{SC} \quad (7)$$

where L_C represents the average change rate of TCB relative to TCG, and $P(TT) - P(T_0)$ can be calculated according to the corresponding time ephemeris.

v. TCB→TDB

$$TDB - TCB = -L_B \times (\mathrm{JD}_{TCB} - T_0) \times 86,400 + TDB_0 \quad (8)$$

where L_B represents the average rate of change in TDB relative to TCB.

The final value obtained by $TDB-TT$ is the delay generated by the time scale transformation, which is the Einstein delay term in Formula (1). It can be found that there are differences in the conversion process between *TCG* and *TCB* (when two quasi-inertial system coordinates) due to the use of different ephemerides; in general, the higher the ephemeris accuracy, the more accurate the calculated delay. For the values of the above constants, there are slight differences in different ephemerides; for example, $L_C^{TE200} = 1.48082685703 \times 10^{-8}$, $L_C^{TE405} = 1.48082685594 \times 10^{-8}$ (the difference value is 1.09×10^{-17}, superscript TE200 and TE405, respectively, represent the time ephemeris calculated based on DE200 and DE405).

The International Earth Rotation Service (IERS) released the time ephemeris TE200 and TE405, but the delay of DE421 and DE430 needs to be obtained by integration according to Formula (5). Table 1 shows the values at different time scales and the Einstein delay of the start time of the observation data (using the coordinate value corresponding to the time of XPNAV-I) calculated according to the four ephemerides. Figure 1 shows the difference between the Einstein delay calculated by DE200 at the initial moment of the 35 groups of photon recording files and the corresponding values of the other three ephemerides.

It was found that the ephemeris has little influence on the calculation of the Einstein delay. During the data observation period adopted in this paper, the difference between the Einstein delays calculated by each ephemeris is less than 1 ns, among which the difference between DE405, DE421 and DE430 is smaller, and the difference between the latest two ephemeris DE421 and 430 is less than 10^{-10} s. In reference [30], the long-term difference between TE200 and TE405 time ephemeris was analyzed, and the maximum difference was less than 5 ns in this century. The celestial mass parameters used in the above results are the actual parameters of each ephemeris. If unified mass parameters are adopted, the difference value will be smaller.

Table 1. Comparison of Einstein delay at satellite at observation start time. The satellite began to observe the Crab pulsar at 8 a.m. UTC time on 17 November 2016.

	UTC	***TT***	***TCG***	***TCB***	***TDB***	**Δ*E***
DE200	8:00:00	8:01:08.184	8:01:9.061046718583	8:01:27.695296538761	8:01:8.182794784679	−0.0012052153210
DE405	8:00:00	8:01:08.184	TCG_{DE200} + 0.0 s	$TCB_{DE200} + 4.47 \times 10^{-10}$ s	$TDB_{DE200} + 4.48 \times 10^{-10}$ s	$\Delta E_{DE200} + 4.480 \times 10^{-10}$ s
DE421	8:00:00	8:01:08.184	TCG_{DE200} + 0.0 s	$TCB_{DE200} + 5.06 \times 10^{-10}$ s	$TDB_{DE200} + 5.06 \times 10^{-10}$ s	$\Delta E_{DE200} + 5.063 \times 10^{-10}$ s
DE430	8:00:00	8:01:08.184	TCG_{DE200} + 0.0 s	$TCB_{DE200} + 5.13 \times 10^{-10}$ s	$TDB_{DE200} + 5.14 \times 10^{-10}$ s	$\Delta E_{DE200} + 5.135 \times 10^{-10}$ s

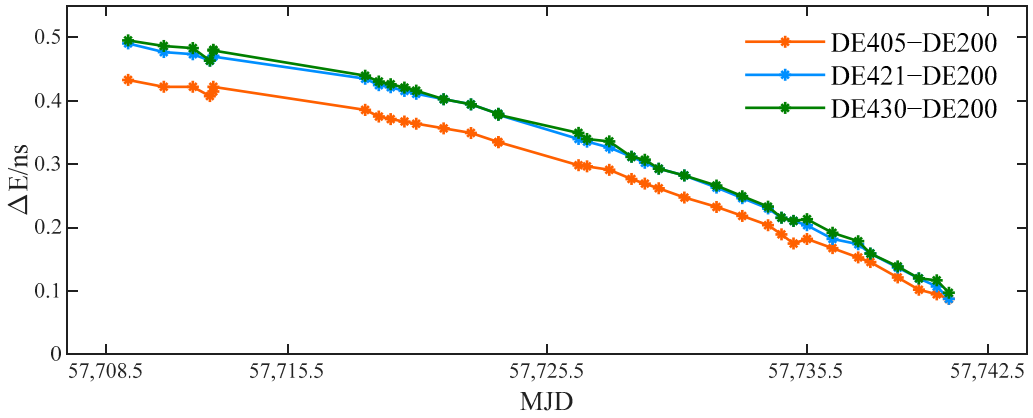

Figure 1. Comparison of Einstein delay during data observation. To clearly reflect the small difference in Einstein delays during observation, subtract DE200 Einstein delay from DE405, 421 and 430 Einstein delays, respectively. The orange curve "DE405–DE200" in the figure represents $\Delta E_{DE405} - \Delta E_{DE200}$; the blue curve represents $\Delta E_{DE421} - \Delta E_{DE200}$; the green curve represents $\Delta E_{DE430} - \Delta E_{DE200}$.

2.2. Effect on Light-Travel Delay

After the time scales at the spacecraft and SSB are unified, the spatial light-travel delay can be calculated according to the geometric relationship between them, that is, ΔR, ΔS and ΔP in Formula (1) (observation formula in pulsar navigation or timing). Formula (9) is the solar system light-travel delay for X-ray pulsar observation [5,10,12]

$$\begin{aligned} t_{SSB} - t_{SC} = {} & \tfrac{n\cdot r}{c} + \tfrac{1}{cR_0}[v\cdot r - (n\cdot v)(n\cdot r)]\Delta t - \tfrac{1}{cR_0^2}(n\cdot v)[v\cdot r - (n\cdot v)(n\cdot r)]\Delta t^2 \\ & - \tfrac{1}{2cR_0}\left[(r)^2 - (n\cdot r)^2\right] + \sum_{k=1}^{N} \tfrac{2GM_k}{c^3}\ln|n\cdot r_k + r_k| - \tfrac{4G^2M_S^2}{c^5 r_s \tan\psi \sin\psi} \end{aligned} \tag{9}$$

where n is the unit vector of the pulsar in the Barycentric Celestial Reference System (BCRS); r is the position vector of the satellite relative to the SSB at the time of observation; v is the velocity vector of the pulsar relative to SSB; $\Delta t = t - t_0$ is the difference between the observation time and the reference epoch; R_0 is the distance between the pulsar and the SSB at the reference epoch; G is Newton's gravitational constant and M_k is the mass of the kth solar system celestial body; r_k is the position vector of the satellite relative to the kth solar system celestial body at the observation time, and r_k is the modulus of r_k; N is the number of solar system celestial bodies for which Shapiro delay is to be calculated; r_s is the distance from the satellite to the Sun at the observation time; M_S is the solar mass; ψ is the angle of the Sun and pulsar relative to the satellite at the observation time. The descriptions of the items on the right side of Formula (9) are as follows:

i. Solar system Roemer delay

The solar system Roemer delay includes the geometric delay term caused by the spacecraft position and the pulsar proper motion. Now define r_P to represent the projection of the vector r in the n direction, that is, $r_P = n\cdot r$; r_V represents the vector perpendicular to n, $r_V = r - r_p n$. If the pulsar 3D proper motion is assumed to be constant, i.e., $v\Delta t \equiv l$, and the items with delay less than 1 ns are ignored, the Roemer delay can be simplified as

$$\Delta R = c^{-1} r_P + c^{-1} R_0^{-1} l_V \cdot r_V - c^{-1} R_0^{-2} l_P l_V \cdot r_V \tag{10}$$

where the first item of the above formula corresponds to the first item on the right of Formula (9), which represents the zero-order Roemer delay caused by the radial position motion of the spacecraft. The second item corresponds to the second item of Formula (9), which is the time delay of the solar system caused by the pulsar radial proper motion. The third item corresponds to the third item of Formula (9), which is the second-order Roemer delay of the solar system caused by the transverse direction induced by radial motion and can be regarded as the correction of the second item.

ii. Solar system Parallax delay

Parallax delay corresponds to the fourth item on the right side of Formula (9), which is the curvature delay term caused by the inconsistency of radial components caused by the position change of the spacecraft during continuous observation, which can be simplified as

$$\Delta P = -\frac{1}{2}c^{-1}R_0^{-2}r_V^2 \tag{11}$$

iii. Solar system Shapiro delay

The fifth and sixth items on the right side of Formula (9) represent the first-order and second-order Shapiro delay of the solar system, respectively, which are the relativistic effect delay caused by the space-time curvature caused by the gravitational field of all celestial bodies in the solar system. If only the gravitational delay caused by the Sun is considered, the relevant items can be simplified as follows

$$\Delta S = \frac{2GM_S}{c^3}\ln|r_{SP} + r_S| - \frac{4G^2M_S^2}{c^5 r_s \tan\psi \sin\psi} \tag{12}$$

It was found that each item of calculating light-travel delay involves the use of ephemeris, so the influence of ephemeris is particularly significant. For near-Earth satellite or ground-based radio observations, the spatial delay error caused by the Earth ephemeris error and the relativistic effect caused by massive celestial bodies such as the Sun and Jupiter is the error items that must be considered. A large error leads to the inability to extract the pulse profile that conforms to the periodic sequence. Table 2 shows the delay items of the XPNAV-I satellite at the start time of observation calculated based on four ephemerides. Figure 2 shows the difference between the light-travel delay calculated by the DE200 at the initial moment of the 35 groups of photons recording files and the corresponding values of the other three ephemerides.

Table 2. Comparison of start time delay of observation data (unit: s, UTC: 2016.11.18 08:00:00.0).

	Roemer	Parallax	Shapiro	Light-Travel Delay
DE200	−433.639869983242	$2.28207289 \times 10^{-27}$	$-2.59819521802 \times 10^{-4}$	−433.640129802764
DE405	$\Delta R_{DE200} + 1.355447560 \times 10^{-3}$	$\Delta P_{DE200} + 5.39 \times 10^{-32}$	$\Delta S_{DE200} - 6.60 \times 10^{-13}$	$\Delta L_{DE200} + 1.355447560 \times 10^{-3}$
DE421	$\Delta R_{DE200} + 1.359091856 \times 10^{-3}$	$\Delta P_{DE200} + 5.39 \times 10^{-32}$	$\Delta S_{DE200} - 6.85 \times 10^{-13}$	$\Delta L_{DE200} + 1.359091856 \times 10^{-3}$
DE430	$\Delta R_{DE200} + 1.358951972 \times 10^{-3}$	$\Delta P_{DE200} + 5.39 \times 10^{-32}$	$\Delta S_{DE200} - 6.91 \times 10^{-13}$	$\Delta L_{DE200} + 1.358951972 \times 10^{-3}$

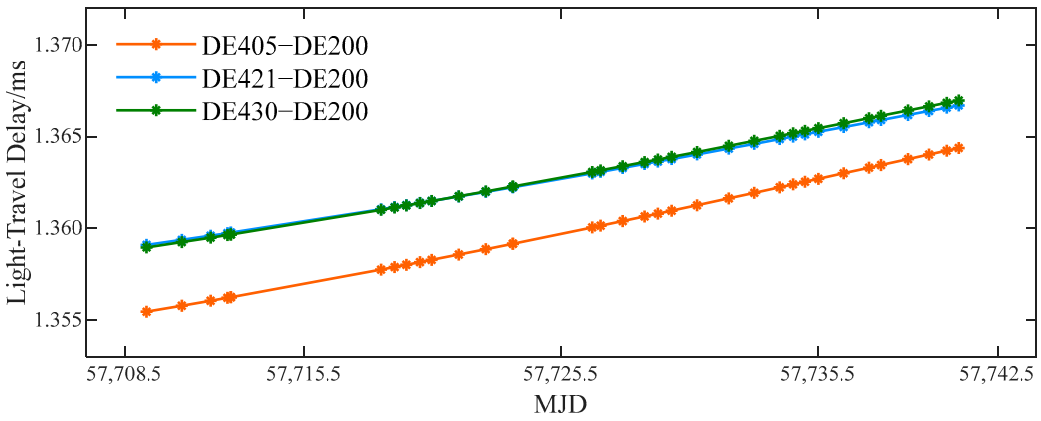

Figure 2. Comparison of time delay during data observation. The meaning of each curve is the same as that in Figure 1, and "DE405-DE200" represents the difference between the light-travel delay calculated by DE405 and DE200, and the rest are analogous.

By comparing the results, it was found that Roemer delay is the main component of light-travel delay and the delay with the largest difference in calculation results between

different ephemerides. The difference between the Roemer delay calculated based on DE200 and the values of the other three ephemerides is greater than 1 ms. The difference between Roemer delay calculated by DE405, DE421 and DE430 is less than 10 μs. The difference between the two latest ephemeris Roemer delay is 0.1 microsecond. The ephemeris has little effect on parallax delay and Shapiro delay, and the difference between the results is in the order of picoseconds.

By comprehensively comparing Figures 1 and 2, it can be found that the time difference shows a linear trend as a whole during the observation period, but the difference between Einstein delay in Figure 1 shows a small jump at a few points, which may be related to the change in satellite position (or there is some error in the satellite position files). It is a pity that this paper does not compare the long-term change trend of the difference, but the simulation analysis of similar satellites shows that Figures 1 and 2 conform to the long-term change trend.

2.3. Comprehensive Impact Analysis on Timing Results

After time scale conversion and light-travel delay calculation of the original photons sequence observed by the spacecraft, the phase of the corresponding time can be calculated according to the periodic information of the observed pulsar. The phase calculation formula is the following Taylor expansion [31]:

$$\varphi(t) = \varphi_0 + f_0(t - t_0) + \frac{1}{2}\dot{f}_0(t - t_0)^2 + \frac{1}{6}\ddot{f}_0(t - t_0)^3 + \cdots \tag{13}$$

where t_0 is the reference epoch; φ_0 is the rotation phase of the reference epoch; f_0, $\dot{f}_0$ and $\ddot{f}_0$ are the rotation frequency and its first and second derivatives. After calculating the phase, the pulse profile in the observation period can be obtained according to the epoch folding method. By comparing the folded pulse profile p with the standard pulse profile $\widetilde{p}$, the phase delay of the pulse can be obtained, and then the initial phase can be obtained. The cross-correlation method is the most commonly used phase comparison method at present. For discrete pulse, its cross-correlation function is:

$$R_D(\varphi) = \frac{1}{N_b}\sum_{i=1}^{N_b} p_i \widetilde{p}_{i+\varphi} \tag{14}$$

where φ is the phase difference between two profiles; N_b is the number of pulse bins. The phase delay shall maximize the cross-correlation function. If the starting point of the folding period is the starting point of the observation period, the estimation of the initial phase is:

$$\widetilde{\varphi}_0 = \underset{\varphi\in[0,1)}{\operatorname{argmax}} R_D(\varphi) \tag{15}$$

Based on the above analysis, it was found that the ephemeris is an important variable to be considered in time scale conversion and spatial light-travel delay calculation, and its influence does not need to be considered too much in phase calculation and phase comparison. In the actual timing applications, if the actual period of pulsars is not searched according to the photon sequence, but the timing parameters published by some institutions (including period, phase and its derivatives), it is necessary to pay attention to the ephemeris used in the data. For example, the Crab timing parameters published by the British Jodrell Bank Observatory use DE200, and the ephemeris used for similar data of the Australian Telescope National Facility (ATNF) is DE405 [32,33]. The mixing of several ephemerides in the timing process may produce a certain systematic deviation.

3. Effect of Ephemeris on Satellite Navigation and Orbit Determination

According to the traditional navigation and positioning theory, in Formula (9), if the timing result on the right side is known, r can be calculated iteratively. Without considering the clock difference, the absolute spatial positioning can be achieved by observing three

pulsars simultaneously [10,12]. However, considering the limited relevant research at present, there is no space experiment using this ideal model for navigation verification. In general, a single detector can be used to observe a pulsar for a long time, and the satellite orbit can be determined based on the orbital-dynamics theory, or a single detector sequentially observes multiple pulsars and then synchronizes the observations to the same epoch, which can also achieve positioning in theory. A similar approach was used in a successful verification experiment conducted by NASA in 2018 [11].

Considering the influence of ephemeris, if the first model is applied, its influence is similar to pulsar timing, and the error value it generates in the positioning equation can be calculated according to the law of error propagation. Wang and Xu et al. conducted some research and analysis on this. For the single satellite observation model, considering that the observation period is generally long, it is difficult to model the error caused by the ephemeris, but it is also possible to conduct experiments to compare the effects of different ephemerides on the final orbit determination results to make an effective evaluation of the ephemeris.

3.1. Positioning Error Modeling

Combined with the analysis of reference [22,23], considering the systematic deviation caused by ephemeris error, the measurement model of the X-ray pulsar navigation system can be modified as:

$$\Delta\tau_{SC} = \Delta\tau + \sum_{k=1}^{N} \frac{B_k}{c} + \frac{\Delta\varepsilon}{c} \tag{16}$$

where $\Delta\tau_{SC}$ is the difference between the measured TOA and the predicted TOA, and $\Delta\tau$ is the time delay caused by the deviation of the real position of the satellite; B_k is the systematic deviation caused by the ephemeris error of the kth planet or celestial body (the serial number similar to the JPL ephemeris), and N is the number of celestial bodies considered; $\Delta\varepsilon$ is the time delay caused by other measurement errors. The specific expression of B_k is related to the actual navigation situation and the influence quantity of the celestial body, which can be derived from the timing formula.

The basis of the analysis in this paper is to know the position error of celestial bodies in three-dimensional space coordinates s and analyze them one by one. However, to achieve high-precision timing or positioning, the disturbance of large mass celestial bodies and even some asteroids in the solar system needs to be considered. Moreover, the comprehensive influence of various errors is not a simple linear superposition but a nonlinear system problem. In order to illustrate its impact, more in-depth research is needed.

3.2. Effect of Ephemeris on Single Pulsar Navigation or Orbit Determination

Considering the limited observation data of X-ray pulsar and the immature navigation technology, the orbit determination of detector based on single X-ray pulsar observation data combined with spacecraft orbit dynamics model has certain application value in the verification of X-ray pulsar navigation theory and the performance test of the detector. For near-Earth satellites, the kinematic equation of spacecraft in an inertial coordinate system is [34]:

$$\ddot{r}_{SC/E} = F\left(t, r_{SC/E}, \dot{r}_{SC/E}, p\right) = -\frac{GM_e}{r_{SC/E}^3} r_{SC/E} + \ddot{R}\left(t, r_{SC/E}, \dot{r}_{SC/E}, p\right) \tag{17}$$

where $r_{SC/E}, \dot{r}_{SC/C}$ and $\ddot{r}_{SC/E}$ are the position, velocity and acceleration vectors of the spacecraft relative to the Geocentric Celestial Reference System (GCRS) at time t, respectively; p is the kinetic model parameter adopted. The position vector of spacecraft in BCRS can be deduced from $r_{SC/E}$ and ephemeris, that is, r in Formula (9). The two formulas can be combined to solve the position vector according to the pulsar timing observations. The principal term of the formula of motion is the two-body motion of the first item on the right side; the second item represents the sum of the perturbation accelerations acting on the

spacecraft, in which the gravitational perturbation produced by some celestial bodies is a non-negligible amount.

In most dynamic orbit determination analyses and experimental simulations, pulse TOA is still taken as the observation measurement. However, for most detectors, including XPNAV-I, the observation pulse with a high signal-to-noise ratio (SNR) cannot be obtained in a short time, so a stable and continuous TOA observation measurement cannot be obtained. In order to solve this problem, an autonomous orbit determination algorithm based on normal plane constraint was proposed in reference [17], and the navigation test was carried out by using the three-month Crab observation data of XPNAV-I; the accuracy of orbit determination at the control point was 38.4 km. Since most of the published data were distributed in December 2016, the line-of-sight direction of the pulsar is almost perpendicular to the satellite orbit plane, which is not conducive to the orbit correction of this method.

Considering the observational characteristics of the experimental data, the pulsar navigation method "Significance Enhancement of Pulse-profile with Orbit-dynamics" (SEPO) in reference [18] was adopted, instead of selecting the pulse TOA as the measurement for pulsar navigation, the observed pulse profile was directly analyzed. Since the pulse profile and the orbit are closely coupled, and the simulated profile is highly similar to the actual profile and is also modulated by the orbit, the deformation of the profile can reflect the significant change in the orbit. The significance χ^2 of the pulse profile is defined as follows:

$$\chi^2 = \sum_i^{N_b} \frac{(\overline{p}_i - \widetilde{p}_i)^2}{\widetilde{p}_i} \tag{18}$$

among them, $\overline{p}_i$ is the pulse profile generated by simulation, and $\widetilde{p}_i$ is the standard pulse profile of the original observation data. When the predicted orbit is closer to the real orbit, the closer the pulse profile is to the real profile, and the greater the significance χ^2 is. Zheng et al. applied this method to the orbit determination analysis of high-energy space detectors such as POLAR of TG-2 space station, Insight-HXMT Satellite, etc., and verified the effectiveness of this method [18,19].

4. Experimental Results and Discussion

The above mainly expounds on the commonly used X-ray pulsar navigation and timing methods. When analyzing the influence of ephemeris on timing, the differences in different ephemerides used in time scale and optical delay calculation are analyzed based on XPNAV-I observation data. By using the same data, this section mainly calculates and compares the effects of different ephemerides on pulse profile, timing residuals and single pulsar orbit determination and gives some suggestions on the use of ephemeris based on the results.

4.1. Pulse Profile

The pulse profile is obtained by the epoch folding method, and the timing parameters are the crab timing parameters regularly released by Jodrell Bank Observatory. (In order to minimize timing noise, it is necessary to use parameters that are as consistent as possible with the date of the observed data. During the observation period, 2016/11/17~12/19, Jodrell has the data of reference epoch 11/23 and 12/16, while the reference epoch of ATNF similar data is very old. See Appendix A Table A3 for details) The standard pulse profile obtained from all 35 groups of observation data is shown in Figure 3.

It can be found that there is a certain systematic deviation between the standard profile obtained by DE200 and the profiles obtained by the other three ephemerides. The calculated deviation value is about 1.3 ms. The deviation value is approximately equal to the timing deviation of each ephemeris; the difference between the profiles obtained by DE405, 421 and 430 is small, and the photon number difference of discrete phase points is generally less than 100. Due to the small number of profile bins, the systematic deviation between the three cannot be displayed through the profiles. For the systematic deviation between the

DE200 profile and the other three, the possible reason for the deviation is that the DE200 is transformed from the B1950 coordinate system to the J2000 coordinate system through coordinate transformation according to the older ephemeris, while the newer ephemeris is compiled according to the latest observation data at that time and based on ICRF. The two methods are likely to produce some spatial deviations.

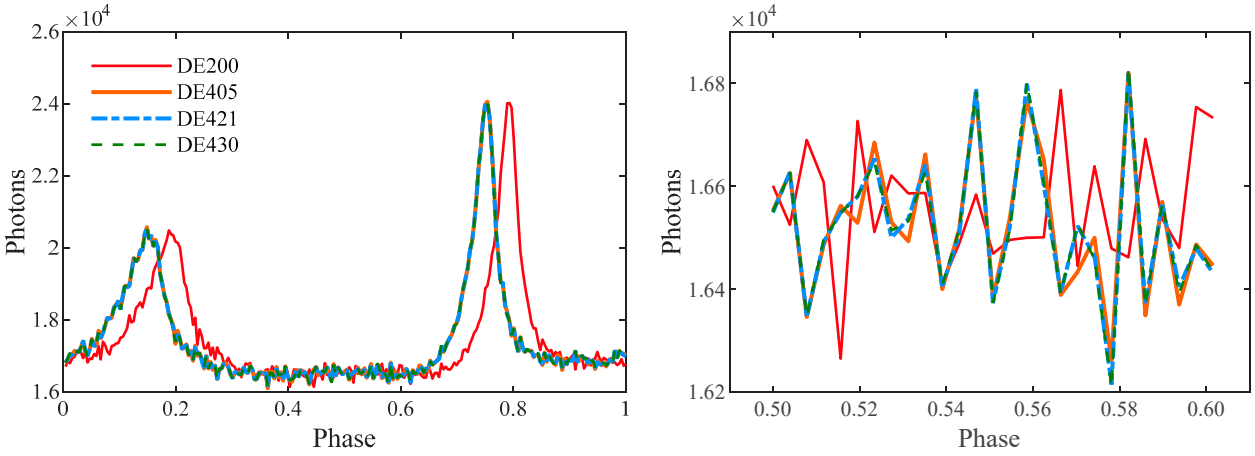

(**a**) Integral period profiles (**b**) Partial period profiles.

Figure 3. Comparison of standard pulse profiles. The number of profile bins is 256. The profiles of DE405, DE421 and DE430 in (**a**) basically coincide. (**b**) shows the profile difference during the period of phase value 0.5–0.6 (it can more clearly reflect the photon number differences of the profiles in this interval).

If the systematic deviation of the DE200 profile relative to the other three is corrected, the resulting standard pulse profile is shown in Figure 4. The Pearson correlation coefficient between each profile is calculated according to the profiles after error correction, as shown in Table 3.

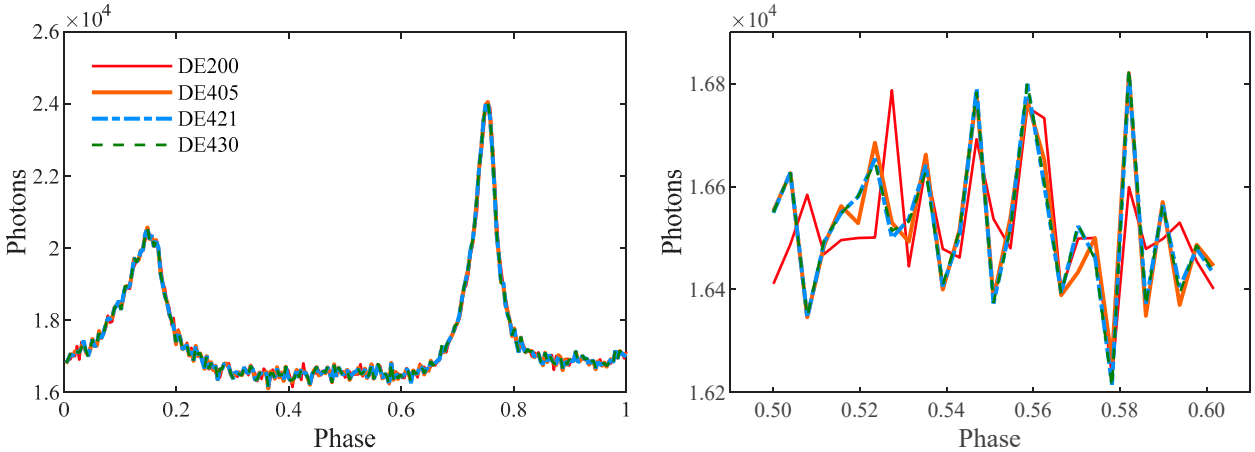

(**a**) (**b**)

Figure 4. Comparison of standard pulse profiles after correcting system deviation. (**a**) Integral period profiles; (**b**) Partial period profiles.

Table 3. Pearson correlation coefficient between pulse profiles. P_200_405 represents the Pearson correlation coefficient between DE200 profile and DE405 profile, and the rest are analogous.

Ephemerides	P_200_405	P_200_421	P_200_430	P_405_421	P_405_430	P_421_430
Pearson_corr	0.996272152	0.996293838	0.996299275	0.999859096	0.999860405	0.999991201

It can be found that the difference between the profiles is small after correcting the system deviation, and the Pearson correlation coefficients between the profiles are higher than 0.99. The profiles of DE200 can still see obvious photon number differences at some discrete phase points. The profiles of the two latest ephemerides almost coincide, and the photon number difference at most discrete phase points is less than 10.

4.2. Timing Residuals

Each group of observation data was folded to obtain a pulse profile, and its phase starting point is the phase corresponding to the arrival time of the first photon of the data, and then the phase difference was obtained by cross-correlation operation with the standard pulse profile. Without considering the integer ambiguity, the obtained phase difference is the normalized phase delay, and the difference between the phase calculated by the standard timing parameters and multiplied by the period is the timing residual. Here, the fast Fourier transform (FFT) was used to calculate the cross-correlation, and the timing residuals calculated based on each ephemeris are shown in Figure 5. Table 4 shows the corresponding RMSE and MAE values.

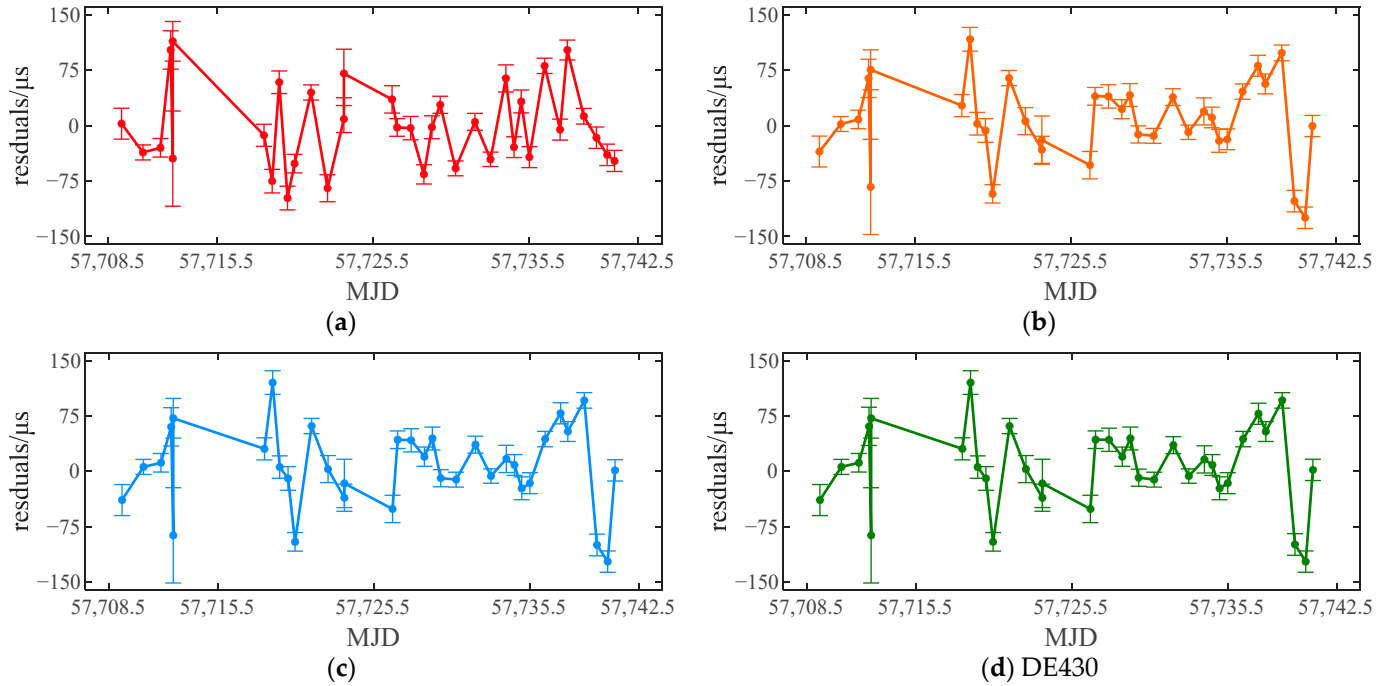

Figure 5. Comparison of timing residuals. The vertical line in the figure represents the mean square error of timing. (**a**) DE200; (**b**) DE405; (**c**) DE421; (**d**) DE430.

Table 4. Comparison of RMSE and MAE values (unit: μs).

Ephemeris	DE200	DE405	DE421	DE430
RMSE	54.6418	54.9246	54.5714	54.5273
MAE	44.4169	42.4389	42.1759	42.1400

It was found that the timing residuals of each group calculated based on the four ephemerides are less than 150 microseconds, and the RMSE and MAE values are also very close; the difference is less than 2 μs. Similarly, the timing residuals obtained by DE200 are quite different from those obtained by the other three ephemerides (mainly expressed in the timing residuals at a single point); the difference between the timing residuals of each group of the results obtained from DE405, DE421 and DE430 is very small, and their MAE values of is slightly better than that of DE200, indicating that their internal accuracy

is higher. The systematic trend of timing residuals due to different ephemerides is the same as that of time conversion and light-travel delay calculation.

In order to verify the timing performance when different ephemerides are mixed, the timing residuals were obtained by cross-correlation operation between the DE405 standard pulse profile and other groups of pulse profiles obtained from other ephemerides, and the results are shown in Figure 6; Table 5 shows the corresponding RMSE and MAE values.

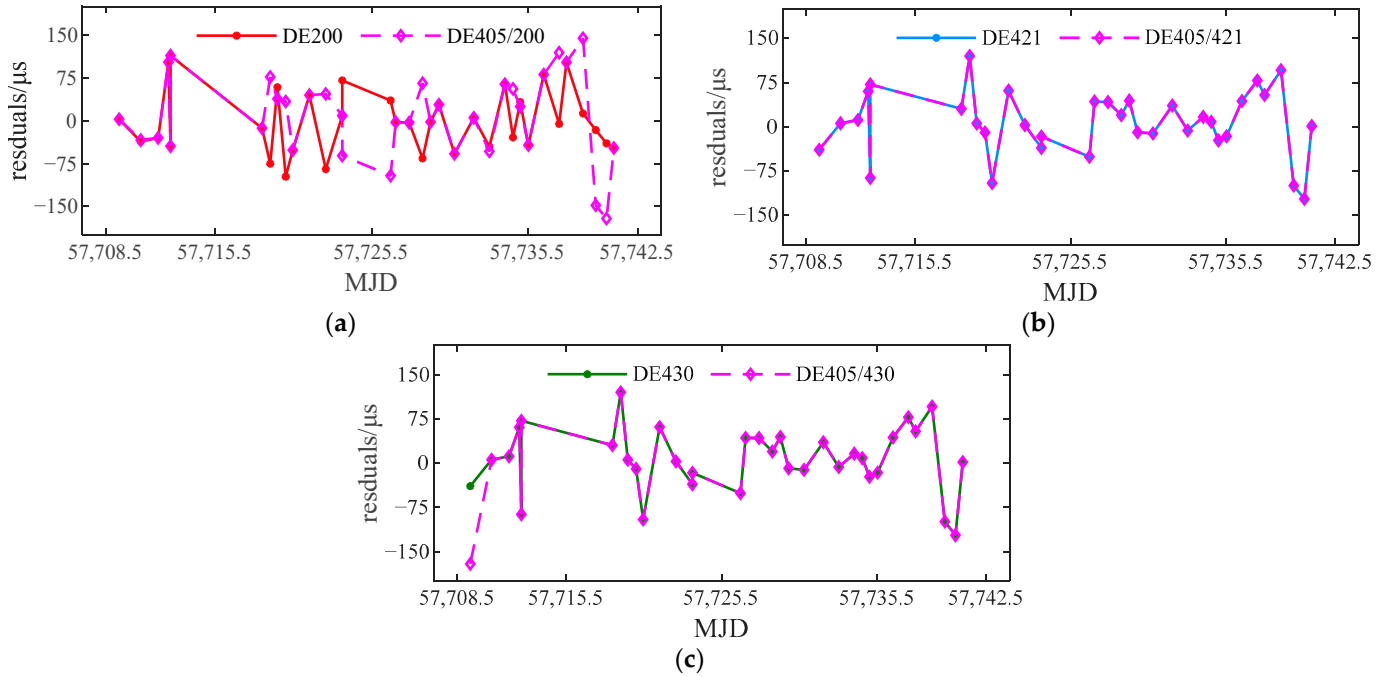

Figure 6. Timing residual using DE405 standard pulse profile. In (**a**), the red curve represents the timing residuals of the original DE200, the purple curve represents the timing residual mixed with the DE200 and standard pulse profile of DE405, and the rest are analogous. (**a**) DE200; (**b**) DE421; (**c**) DE430.

Table 5. Comparison of RMSE and MAE values (unit: μs).

Ephemeris	DE405/200	DE405/421	DE421/430
RMSE	72.2760	54.5714	61.3338
MAE	57.6716	42.1759	45.9044

It was found that the timing residuals obtained by DE405/421 are completely consistent with those obtained by using the DE421 standard profile. Compared with the DE200 standard profile, the timing residuals of DE405/200 increased, the maximum value was more than 150 microseconds, and the values of RMSE and MAE increased by about 30%. The first timing residual of DE405/430 increased significantly, while other values did not change obviously. Affected by the first value, both RMSE and MAE values increased. It can be found that the internal self-consistent ephemeris can generally obtain better results than the mixed ephemerides, which need special attention in the application of pulsar navigation and timing.

4.3. Orbit Determination Analysis

Based on the analysis in Section 2.2, the SEPO was used to analyze the influence of different ephemerides on XPNAV-I orbit determination. In this experiment, the real-time photons arrival rate function at the spacecraft was calculated by using the pulsar signal model at the SSB and the spacecraft orbit information, combined with the pulse

profile of each ephemeris, and then the photons arrival time series was generated by the scale transformation method [35]. The grazing incidence Wolter-I X-ray telescope of XPNAV-I has an area of only 30 cm^2, but it has a small optical field of view and strong noise suppression ability. For one month's sparse observation data, the amount of signal simulation calculation is large.

For each ephemeris, take the GPS coordinate values $[X,\ Y,\ Z]$ recorded by the satellite in the J-2000 coordinate system as the nominal orbit, add errors on the coordinate values in 1 km steps to obtain $[X + \Delta L, Y + \Delta L,\ Z + \Delta L]$, and the ΔL range is $[-10, 10]$ km. Calculate the χ^2 value under each coordinate and determine the range of the optimal orbit according to the size of the χ^2 value. The χ^2 values obtained from different ephemerides are shown in Figure 7 and Table 6 shows the specific values.

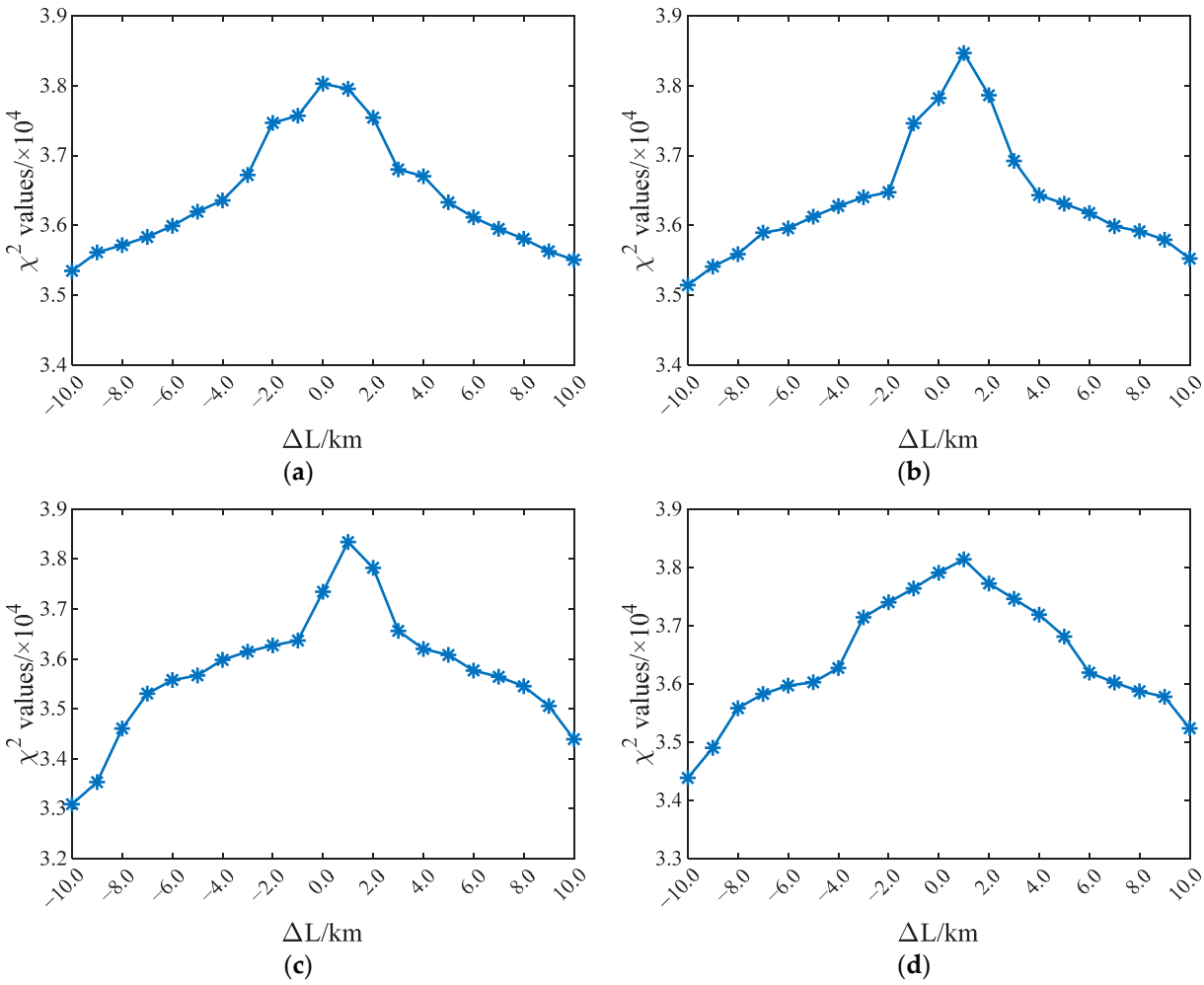

Figure 7. Comparison of chi-square values of each ephemeris simulation orbit. (**a**) DE200; (**b**) DE405; (**c**) DE421; (**d**) DE430.

It was found that for the four ephemerides used, the χ^2 value of the simulation profiles can show a certain regularity rather than random distribution. The peak value represents the deviation between the simulated orbit and the actual orbit. The difference between the orbit obtained by DE200 and the actual orbit is less than 1 km, while the deviation of the other three ephemerides is between 1 and 2 km. Due to the limited experimental data, it is impossible to draw a conclusion that the orbit accuracy of DE200 is higher, which may be that the timing parameters used are the crab timing parameters of Jodrell Bank Observatory compiled based on DE200. Further experimental analysis is needed to draw a more accurate conclusion.

Table 6. χ^2 values of each ephemeris simulation orbit.

Δ*L*/Km	DE200	DE405	DE421	DE430
−10	35,348.58282	35,144.58369	33,088.10955	34,385.1766
−9	35,613.47329	35,409.82768	33,530.0139	34,900.42859
−8	35,717.51518	35,589.39763	34,604.85721	35,581.71327
−7	35,834.13222	35,895.86897	35,304.83125	35,826.32905
−6	35,992.52258	35,956.87852	35,577.09967	35,970.18901
−5	36,195.84801	36,124.38468	35,667.40987	36,026.41001
−4	36,357.96755	36,276.69509	35,980.34176	36,271.05581
−3	36,720.60294	36,402.48305	36,145.60529	37,140.7892
−2	37,465.89581	36,474.49957	36,270.53755	37,401.09154
−1	37,569.36244	37,460.36531	36,368.28404	37,639.15843
0	38,028.23266	37,819.99479	37,344.9412	37,907.62134
1	37,953.4562	38,466.26153	38,340.82654	38,138.94381
2	37,540.49097	37,862.25479	37,824.27274	37,723.94564
3	36,801.20982	36,922.62293	36,561.31364	37,458.42178
4	36,702.71458	36,431.87019	36,199.47831	37,187.3775
5	36,328.88002	36,310.29199	36,078.04842	36,811.37727
6	36,116.18036	36,176.77891	35,766.93906	36,192.90688
7	35,949.24826	35,989.3597	35,641.37276	36,021.83881
8	35,807.98256	35,915.39357	35,451.27367	35,873.25145
9	35,629.80379	35,793.25319	35,055.39206	35,776.89203
10	35,507.51493	35,524.15199	34,390.37655	35,235.99492

It should be noted here that the "orbit determination" analyzed in this paper is to reverse the pulse profile based on the known nominal orbit, and it cannot be used for actual pulsar navigation or orbit determination, but for the research of this paper, it can still reflect the influence of different ephemerides on orbit determination accuracy to a certain extent.

4.4. Discussion

In the pulsar timing calculation, a relatively strict calculation process was adopted, and the results were improved compared with some research results using the same data [7,17]. The timing residuals error of multiple groups of data is less than 50 microseconds, and the corresponding ranging error is less than 15 km. If the corresponding timing accuracy is converted into positioning accuracy, it has satisfied the navigation and positioning requirements of the transfer orbit segment of the deep space explorer. At the same time, how to form an effective timing measurement in a short time is the focus of future research.

Compared with the old ephemeris, the newer ephemeris usually has higher spatial accuracy. Most studies also show that the newly released ephemeris often has better timing performance [6]. The above experimental results also show that when the systematic deviation is corrected, the MAE values of the timing residuals of the three newer ephemerides are still slightly better than that of DE200, indicating that their internal accuracy is higher. For some historical reasons, pulsar timing parameters obtained from older ephemeris such as DE200 are still widely used and of a certain value. In order to adapt to the development of research as soon as possible, it is necessary to use the newer ephemeris to obtain timing parameters and promote them.

In this paper, the orbit determination based on single pulsar observation data was used to analyze the navigation accuracy, which is an ideal processing method in the case of a lack of observation data. It should be noted that the "orbit determination" analyzed here is to reverse the pulse profile based on the known nominal orbit, and it cannot be used for actual pulsar navigation or orbit determination, but for the research of this paper, it can still reflect the influence of different ephemerides on orbit determination accuracy to a certain extent. Later, the same observation data can be used for rigorous dynamic orbit determination analysis.

Compared with the modeling of timing and positioning error caused by ephemeris error in some papers, this paper only calculates the difference of different ephemerides

in timing and navigation solutions [22–24]. However, through analysis, it was found that ephemeris error belongs to red noises that are difficult to model, and the absolute errors of celestial coordinates or velocity in different ephemerides are also difficult to determine, so it may be difficult to deal with its impact in ephemeris error modeling. According to the appeal analysis, on the one hand, the whole process can be solved based on one newly released ephemeris to reduce the impact of the internal inconsistency of ephemeris. On the other hand, with the development of complex system analysis and multi-body motion theory, it can also be introduced into the study of a pulsar navigation system to establish a more accurate model.

Due to the limited observation data, there is no experimental comparison for most navigation or timing situations. Subsequent analysis can be based on ground radio observation data and long-term observation data from other satellites to obtain more accurate conclusions.

5. Conclusions

The effects of JPL DE ephemeris on X-ray pulsar navigation and timing were studied and experimentally analyzed. Firstly, the current theoretical models and data processing methods of X-ray pulsar timing and navigation were summarized and analyzed, and the possible differences of ephemeris in the solution of timing and navigation equations were emphatically analyzed. Based on the measured data released by XPNAV-I, the effects of four commonly used JPL DE ephemerides on timing and orbit determination results were compared, and the following conclusions were summarized:

(1) For time scale conversion, the difference is less than 1 ns during the data recording period, and the long-term difference is also less than 5 ns. The ephemeris has a significant impact on the calculation of light-travel delay. For Romer delay, the difference value can be greater than 1 ms, but for Shapiro delay and other relativistic effects caused by gravity, the delay difference value is small. At the same time, with the update and standardization of the ephemeris, the difference value was very small;

(2) For the final timing results, the profile obtained by DE200 has a certain systematic deviation compared with other ephemerides, which is approximately equal to the delay difference, and the difference between RMSE and MAE values of timing residuals calculated by each ephemeris is less than 2 μs. However, the cross-correlation operation of the pulse profile obtained from different ephemerides increases the timing residuals. Therefore, when using ephemeris in navigation and timing applications, we must pay attention to its internal self-consistency;

(3) When the four ephemerides are used for orbit determination, the orbit differences value is less than 1 km. Since the timing parameters are calculated based on DE200, its navigation or orbit determination accuracy is more accurate than the other three ephemerides, which also shows the importance of adopting a unified ephemeris in all links. At the same time, considering the higher spatial accuracy of the new ephemeris, it is the future development trend to use it to compile and popularize the pulsar timing model as soon as possible.

Author Contributions: Writing—review and editing, Y.D. and S.J. All authors have read and agreed to the published version of the manuscript.

Funding: This work was supported by the National Key Research and Development Program (Grant No.: 2021YFA0716100).

Institutional Review Board Statement: Not applicable.

Informed Consent Statement: Not applicable.

Data Availability Statement: Data available on reasonable request to the authors.

Conflicts of Interest: The authors declare no conflict of interest.

Appendix A

The four JPL de ephemerides were used in this paper; DE200 was published in 1981, and it was used to compile the American Ephemeris and Nautical Almanac from 1984 to 2003. The timing parameters of Crab pulsar at Jodrell Bank Observatory used in this paper take this ephemeris as the time-space reference; DE405 was released in 1995. Most astronomical yearbooks, including IAU resolutions (2006), IERS Conventions (2003) and the Standards of Fundamental Astronomy (SOFA) software libraries, have been compiled with reference to this ephemeris, and most pulsar parameters released by ATNF also take this ephemeris as the space-time reference; DE421 was released in 2008 and fitted the latest planetary and lunar observation data at that time. At present, most pulsar navigation and timing studies use this ephemeris; DE430 was released in 2013. The latest International Celestial Reference Framework (ICRF2.0) has been used in the compilation of American Ephemeris and Nautical Almanac since 2015. Appendix A Table A1 is a partial introduction to the four ephemerides [20,21].

Table A1. Basic introduction of four ephemerides.

	DE200	DE405	DE421	DE430
Reference Frame	J2000.0	ICRF	ICRF	ICRF2.0
Time Span	JED2305424.5–JED 2513360.5 (AD1599–AD2169)	JED 2305424.5–JED2525008.5 (AD1599–AD2201)	JED 2414864.5–JED 2471184.5 (AD1899–AD2053)	JED2287184.5–JED2688976.5 (AD1549–AD2650)
Observation Data	Radar, Spacecraft	Radar, Spacecraft, CCD, RATE, Transit, Astrolabe	LLR, Radar, Spacecraft, CCD, Photo, Transit	LLR, Spacecraft, Radar, Astrometric, Occultation
Note	Including Nutation but excluding Libration	Including Nutation and Libration	Including Nutation and Libration	Including Nutation and Libration (1980 series)

The XPNAV-I was Launched in November 2016, and it is the world's first dedicated pulsar navigation test satellite, equipped with a collimated microchannel plate detector and a grazing incidence Wolter-I X-ray detector. In May 2017, the Beidou official website released the data of Crab pulsar (PSR B0531+21) observed by the Wolter-1 detector. The basic information of the data is shown in Appendix A Table A2 [28].

Table A2. Statistics of Crab observation data.

Parameter	Value
Start time	UTC 2016/11/17(MJD:57,709.5)
End time	UTC 2016/12/19(MJD:57,741.5)
Number of observation orbits	125
Effective observation duration	366,720 s
Number of detected photons	4,438,661 counts
Source Flux	1.0 counts/s
Background Flux	14.2 counts/s

The basic parameters of the detector are given in the data description file given on the official website. Appendix A Table A3 shows the timing parameters of the Crab pulsar of the Jodrell Bank Observatory [32].

Table A3. Timing parameters of Crab pulsar.

Timing Parameter	Value 1	Value 2
Right ascension (J2000)	05 h 34 m 31.972 s	05 h 34 m 31.972 s
Declination (J2000)	+22°00′52.07″	+22°00′52.07″
Reference epoch TDB	2016/11/23 12:00:01.025488 MJD:57715.000000295	2016/12/16 12:00:01.0200448 MJD:57738.000000232
Time range	57,707~57,723 2016/11/15~12/01	57,723~57,754 2016/12/01~2017/01/01
F0 [Hz]	29.6478547478211	29.6471215546085
F1 [Hz/s^{-1}]	-3.68972^{-10}	-3.68942^{-10}
F2 [Hz/s^{-2}]	-3.89^{-20}	1.55^{-20}

References

1. Hewish, A.; Bell, S.J.; Pilkington, J.D.H.; Scott, P.F.; Collins, R.A. 74. Observation of a Rapidly Pulsating Radio Source. In *A Source Book in Astronomy and Astrophysics, 1900–1975*; Harvard University Press: Cambridge, MA, USA, 2013; pp. 498–504.
2. Taylor, J.H. Pulsar timing and relativistic gravity. Philosophical Transactions of the Royal Society of London. *Ser. A Phys. Eng. Sci.* **1992**, *341*, 117–134.
3. Ellis, J.; Lewicki, M. Cosmic String Interpretation of NANOGrav Pulsar Timing Data. *Phys. Rev. Lett.* **2021**, *126*, 041304. [CrossRef] [PubMed]
4. Goncharov, B.; Shannon, R.; Reardon, D.; Hobbs, G.; Zic, A.; Bailes, M.; Curyło, M.; Dai, S.; Kerr, M.; Lower, M. On the evi-dence for a common-spectrum process in the search for the nanohertz gravitational-wave background with the Parkes Pulsar Timing Array. *Astrophys. J. Lett.* **2021**, *917*, L19. [CrossRef]
5. Edwards, R.T.; Hobbs, G.; Manchester, R. TEMPO2, a new pulsar timing package–II. The timing model and precision estimates. *Month. Not. R. Astr. Soc.* **2006**, *372*, 1549–1574. [CrossRef]
6. Verbiest, J.P.; Bailes, M.; van Straten, W.; Hobbs, G.B.; Edwards, R.T.; Manchester, R.N.; Bhat, N.; Sarkissian, J.M.; Jacoby, B.A.; Kulkarni, S.R. Precision timing of PSR J0437–4715: An accurate pulsar distance, a high pulsar mass, and a limit on the variation of Newton's gravitational constant. *Astrophys. J.* **2008**, *679*, 675. [CrossRef]
7. Huang, L.; Shuai, P.; Zhang, X.; Chen, S. A new explorer mission for soft X-ray timing—Observation of the Crab pulsar. *Acta Astronaut.* **2018**, *151*, 63–67. [CrossRef]
8. Qing-Yong, Z.; Zi-Qing, W.; Lin-Li, Y.; Peng-Fei, S.; Si-Wei, L.; Lai-Ping, F.; Kun, J.; Yi-Di, W.; Yong-Xing, Z.; Xiao-Gang, L. Space/ground based pulsar timescale for comprehensive PNT system. *Acta Phys. Sin.* **2021**, *70*, 471–483.
9. Downs, G. *Interplanetary Navigation Using Pulsating Radio Sources*; JPL Technical Report 32–1594; NASA: Washington, DC, USA, 1974. Available online: https://ntrs.nasa.gov/citations/19740026037 (accessed on 22 June 2022).
10. Sheikh, S.I.; Pines, D.J.; Ray, P.S.; Wood, K.S.; Lovellette, M.N.; Wolff, M.T. Spacecraft Navigation Using X-Ray Pulsars. *J. Guid. Control. Dyn.* **2006**, *29*, 49–63. [CrossRef]
11. Winternitz, L.B.; Hassouneh, M.A.; Mitchell, J.W.; Price, S.R.; Yu, W.H.; Semper, S.R.; Ray, P.S.; Wood, K.S.; Arzoumanian, Z.; Gendreau, K.C. SEXTANT X-ray Pulsar Navigation Demonstration: Additional On-Orbit Results. In Proceedings of the 2018 SpaceOps Conference, Marseille, France, 28 May–1 June 2018.
12. Zhou, Q.; Ji, J.; Ren, H. The Timing Equation in X-Ray Pulsar Autonomous Navigation. In Proceedings of the China Satellite Navigation Conference (CSNC) 2013 Proceedings, Wuhan, China, 15–17 May 2013; pp. 543–554.
13. Xu, Q.; Fan, X.; Ding, B.; Xu, L.; Liu, N. Adaptive two-stage Kalman filter for X-ray pulsar navigation. In Proceedings of the Seventh Symposium on Novel Photoelectronic Detection Technology and Applications, Kunming, China, 5–7 November 2021; p. 117635K.
14. Xue, M.; Peng, D.; Sun, H.; Shentu, H.; Guo, Y.; Luo, J.; Zhikun, C. X-ray pulsar navigation based on two-stage estimation of Doppler frequency and phase delay. *Aerosp. Sci. Technol.* **2021**, *110*, 106470. [CrossRef]
15. Ely, T.; Bhaskaran, S.; Bradley, N.; Lazio, T.J.W.; Martin-Mur, T. Comparison of Deep Space Navigation Using Optical Imaging, Pulsar Time-of-Arrival Tracking, and/or Radiometric Tracking. *J. Astronaut. Sci.* **2022**, *69*, 385–472. [CrossRef]
16. Lv, Z.; Mei, Z.; Deng, L.; Li, L.; Chen, J. In-orbit calibration and data analysis of China's first grazing incidence focusing X-ray pulsar telescope. *Aerosp. China* **2017**, *18*, 3–10.
17. Huang, L.; Shuai, P.; Zhang, X.; Chen, S. Pulsar-based navigation results: Data processing of the X-ray pulsar navigation-I telescope. *J. Astron. Telesc. Instr. Syst.* **2019**, *5*, 018003. [CrossRef]
18. Zheng, S.; Ge, M.; Han, D.; Wang, W.; Chen, Y.; Lu, F.; Bao, T.; Chai, J.; Dong, Y.; Feng, M.; et al. Test of pulsar navigation with POLAR on TG-2 space station. *Sci. Sin. Phys. Mech. Astron.* **2017**, *47*, 099505. [CrossRef]
19. Zheng, S.; Zhang, S.; Lu, F.; Wang, W.; Gao, Y.; Li, T.; Song, L.; Ge, M.; Han, D.; Chen, Y. In-orbit demonstration of X-ray pulsar navigation with the Insight-HXMT satellite. *Astrophys. J. Suppl. Ser.* **2019**, *244*, 1. [CrossRef]
20. Xue-Mei, D.; Min, F.; Yi, X. Comparisons and Evaluations of JPL Ephemerides. *Chin. Astron. Astrophys.* **2014**, *38*, 330–341. [CrossRef]
21. JPL Planetary and Lunar Ephemerides. Available online: https://ssd.jpl.nasa.gov/planets/eph_export.html (accessed on 22 June 2021).
22. Wang, Y.; Zheng, W.; Sun, S.; Li, L. X-ray pulsar-based navigation system with the errors in the planetary ephemerides for Earth-orbiting satellite. *Adv. Space Res.* **2013**, *51*, 2394–2404. [CrossRef]
23. Xu, Q.; Wang, H.L.; You, S.; He, Y.Y.; Feng, L. Impact of Ephemeris Errors on X-ray Pulsar Navigation. In Proceedings of the 2018 IEEE CSAA Guidance, Navigation and Control Conference (CGNCC), Xiamen, China, 10–12 August 2018; pp. 1–6.
24. Ning, X.; Yang, Y.; Li, Z.; Gui, M.; Fang, J. Ephemeris Corrections in Celestial/Pulsar Navigation Using Time Differential and Ephemeris Estimation. *J. Guid. Control. Dyn.* **2018**, *41*, 1–8. [CrossRef]
25. Fang, H.; Su, J.; Li, L.; Zhang, L.; Sun, H.; Gao, J. An analysis of X-ray pulsar navigation accuracy in Earth orbit applications. *Adv. Space Res.* **2021**, *68*, 3731–3748. [CrossRef]
26. Ge, M.Y.; Zhang, S.N.; Lu, F.; Li, T.P.; Yuan, J.P.; Zheng, X.P.; Huang, Y.; Zheng, S.J.; Chen, Y.P.; Chang, Z.; et al. Discovery of Delayed Spin-up Behavior Following Two Large Glitches in the Crab Pulsar, and the Statistics of Such Processes. *Astrophys. J. Lett.* **2020**, *896*, 55. [CrossRef]
27. Kaplan, G.H. *The IAU Resolutions on Astronomical Reference Systems, Time Scales, and Earth Rotation Models (Draft 4)*; Naval Observatory: Washington, DC, USA, 2005. [CrossRef]

28. XPNAV-I Online Data. Available online: http://www.beidou.gov.cn/yw/xwzx/201710/t20171010_824.html (accessed on 22 June 2021).
29. Petit, G.; Luzum, B. *IERS Conventions (2010)*; Bureau International des Poids et Mesures Sevres: Saint-Cloud, France, 2010.
30. Irwin, A.W.; Fukushima, T. A numerical time ephemeris of the Earth. *Astron. Astrophys.* **1999**, *348*, 642–652.
31. Emadzadeh, A.A.; Speyer, J.L. On Modeling and Pulse Phase Estimation of X-Ray Pulsars. *IEEE Trans. Signal Process.* **2010**, *58*, 4484–4495. [CrossRef]
32. Jodrell Bank Crab Pulsar Ephemeris. Available online: https://www.jb.man.ac.uk/pulsar/crab.html (accessed on 22 June 2021).
33. The ATNF Pulsar Catalogue. Available online: https://www.atnf.csiro.au/research/pulsar/psrcat/ (accessed on 22 June 2021).
34. Mao, Y.; Chen, J.; Song, X. Single X-ray pulsar dynamic orbit determination. *J. Geom. Sci. Technol.* **2010**, *27*, 251–254.
35. Su, J.; Fang, H.; Bao, W.; Sun, H.; Shen, L.; Zhao, L. Fast simulation of X-ray pulsar signals at a spacecraft. *Acta Astronaut.* **2019**, *166*, 93–103. [CrossRef]